

## **Supplementary Information**

### **Simulation and Comparison of the Photovoltaic Performance of Conventional and Inverted Organic Solar Cells with SnO<sub>2</sub> as Electron Transport Layers**

Boudia Mohamed, Qiuwang Wang and Cunlu Zhao\*

MOE Key Laboratory of Thermo-Fluid Science and Engineering, School of Energy  
and Power Engineering, Xi'an Jiaotong University, Xi'an 710049, China

\* Address the correspondence to this author at [mclzhao@xjtu.edu.cn](mailto:mclzhao@xjtu.edu.cn)

**Table S1.a** The thicknesses of the different layers of the conventional structure of binary organic solar cells for optimum efficiency

Layer	Thicknesses (nm)	Materials	Type
ITO	130	Oxides/fto	Contact
PEDOT:PSS	5	Polymers/pedot_pss	HTL
PM6:L8-BO	80	Blends/PM6_D18_L8-BO	Active
SnO <sub>2</sub>	20	Oxides/sno2	ETL
Ag	100	Metal/Ag	Contact

**Table S1.b** The thicknesses of the different layers of the inverted structure of binary organic solar cells for optimum efficiency

Layer	Thicknesses (nm)	Materials	Type
ITO	130	Oxides/fto	Contact
SnO <sub>2</sub>	5	Oxides/sno2	ETL
PM6:L8-BO	80	Blends/PM6_D18_L8-BO	Active
PEDOT: PSS	20	Polymers/pedotpss	HTL
Ag	100	Metal/Ag	Contact

**Table S1.c** The thicknesses of the different layers of ternary organic solar cells for optimum efficiency

Layer	Thicknesses (nm)	Materials	Type
FTO	130	Oxides/fto	Contact
PEDOT:PSS	5	Polymers/pedot_pss	HTL
PM6:D18:L8-BO	80	Blends/PM6_D18_L8-BO	Active
SnO <sub>2</sub>	20	Oxides/sno2	ETL
Ag	100	Metal/Ag	Contact

**Table S2.a** Simulation parameters of Oghma-Nano software for the binary conventional, and inverted PM6:L8-BO structures

Parameters	Value
Electron mobility ( $\mu_e$ )	1.5e-07 m <sup>2</sup> V <sup>-1</sup> s <sup>-1</sup>
Hole mobility ( $\mu_h$ )	1.152e-07 m <sup>2</sup> V <sup>-1</sup> s <sup>-1</sup>
Effective density of free electron ( $N_c$ at 300K)	1e26 m <sup>-3</sup>
Effective density of free hole ( $N_v$ at 300K)	1e26 m <sup>-3</sup>
$n$ to $P$ Recombination rate constant	1.77e-17 m <sup>-3</sup> s <sup>-1</sup>
Free electron ( $n$ ) to Trapped electron ( $n_{trap}$ )	1e-15 m <sup>-2</sup>
Trapped electron ( $n_{trap}$ ) to Free hole ( $P$ )	1e-20 m <sup>-2</sup>
Trapped Hole ( $P_{trap}$ ) to Free electron ( $n$ )	1e-20 m <sup>-2</sup>
Free hole ( $P$ ) to Trapped hole ( $P_{trap}$ )	1e-15 m <sup>-2</sup>
Number of traps ( $N_t$ )	5 Trap
Energy bandgap ( $E_g$ )	1.28 eV
Relative permittivity ( $\epsilon_r$ )	3.0 a.u

**Table S2.b** Simulation parameters of Oghma-Nano software for ternary organic solar cells

Parameters	Value
Electron mobility ( $\mu_e$ )	$1.49\text{e-}07 \text{ m}^2\text{V}^{-1}\text{s}^{-1}$
Hole mobility ( $\mu_h$ )	$1.42\text{e-}07 \text{ m}^2\text{V}^{-1}\text{s}^{-1}$
Effective density of free electron ( $N_c$ at 300K)	$1\text{e}26 \text{ m}^{-3}$
Effective density of free hole ( $N_v$ at 300K)	$1\text{e}26 \text{ m}^{-3}$
$n$ to $P$ Recombination rate constant	$1.15\text{e-}17 \text{ m}^{-3}\text{s}^{-1}$
Free electron ( $n$ ) to Trapped electron ( $n_{\text{trap}}$ )	$1\text{e-}15 \text{ m}^{-2}$
Trapped electron ( $n_{\text{trap}}$ ) to Free hole ( $P$ )	$1\text{e-}20 \text{ m}^{-2}$
Trapped Hole ( $P_{\text{trap}}$ ) to Free electron ( $n$ )	$1\text{e-}20 \text{ m}^{-2}$
Free hole ( $P$ ) to Trapped hole ( $P_{\text{trap}}$ )	$1\text{e-}15 \text{ m}^{-2}$
Number of traps ( $N_t$ )	5 Trap
Energy bandgap ( $E_g$ )	1.29 eV
Relative permittivity ( $\epsilon_r$ )	3.0 a.u

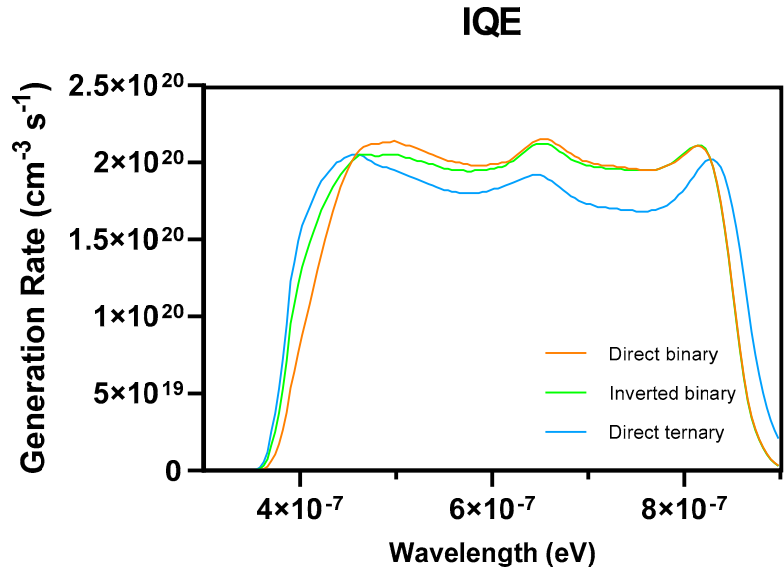


**Figure S1.** Internal quantum efficiency (IQE) of the conventional and inverted binary, and ternary devices

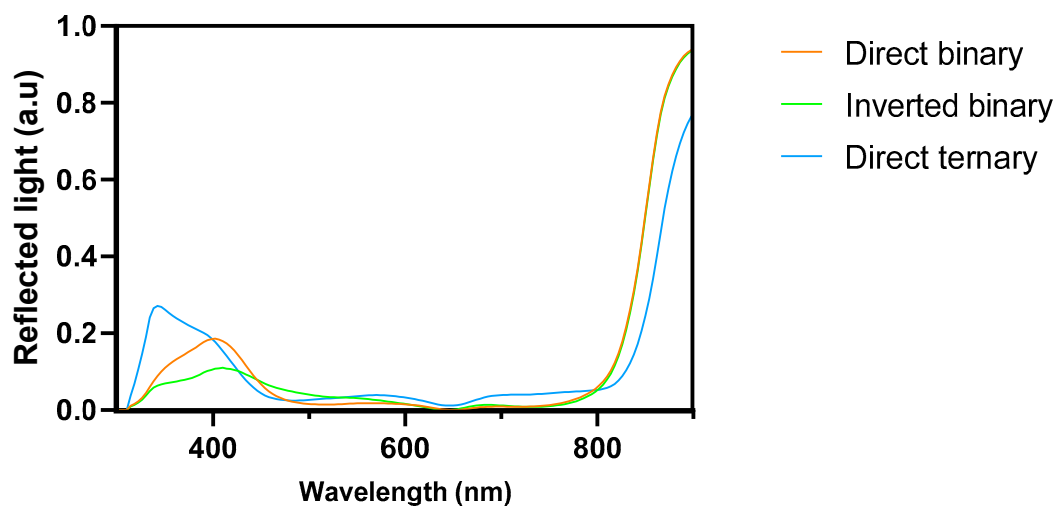


**Figure S2.** The reflected light as a function of the wavelength for conventional and inverted binary, and ternary devices

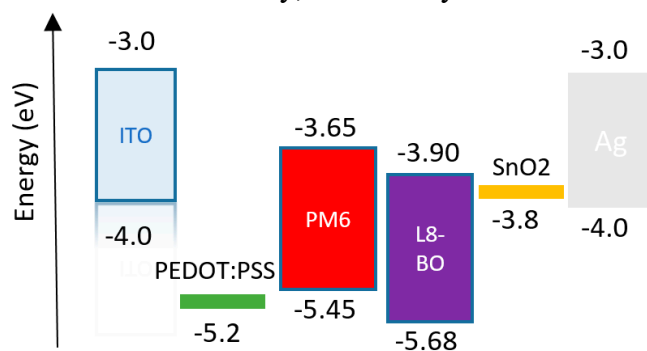


**Figure S3.** Energy levels diagram for Conventional binary organic solar cells

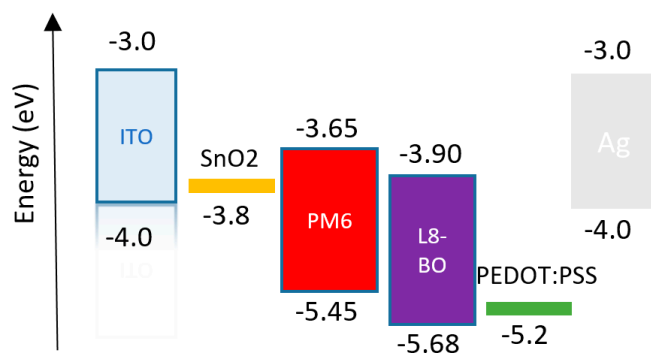


**Figure S4.** Energy levels diagram for Inverted binary organic solar cells

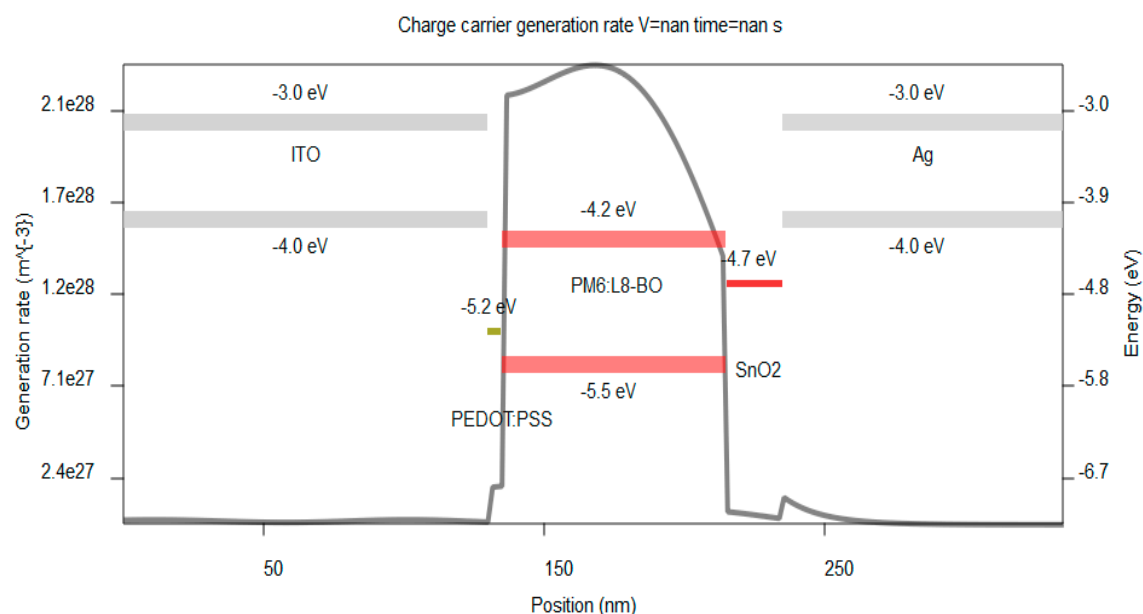


**Figure S5.** Charge carrier generation rate with energy level alignment of different materials of the conventional binary device in function of position

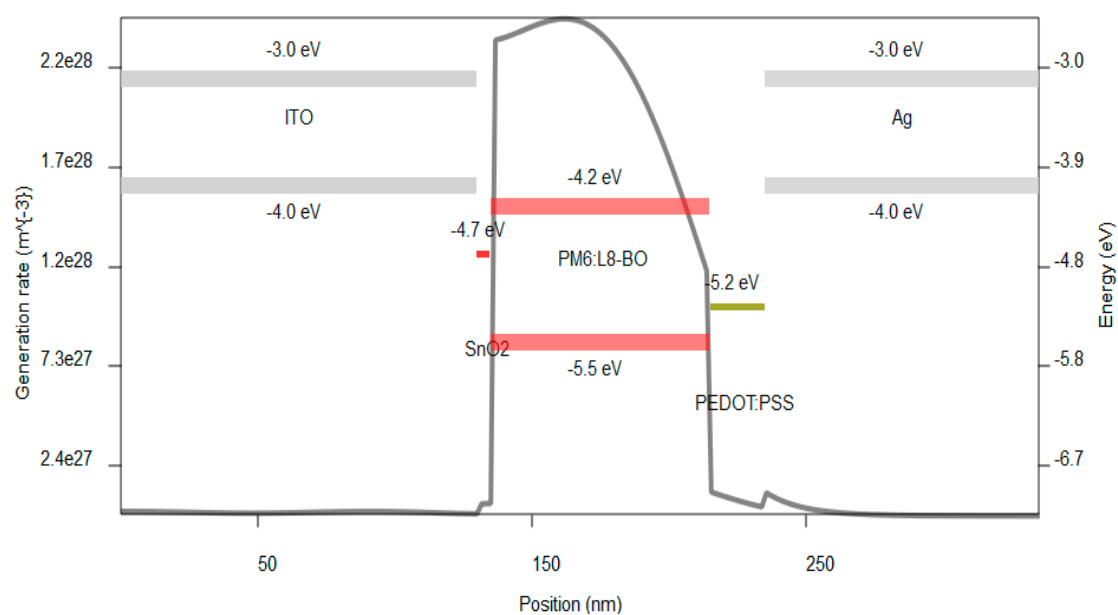


**Figure S6.** Charge carrier generation rate with energy level alignment of different materials of the Inverted binary device in function of position

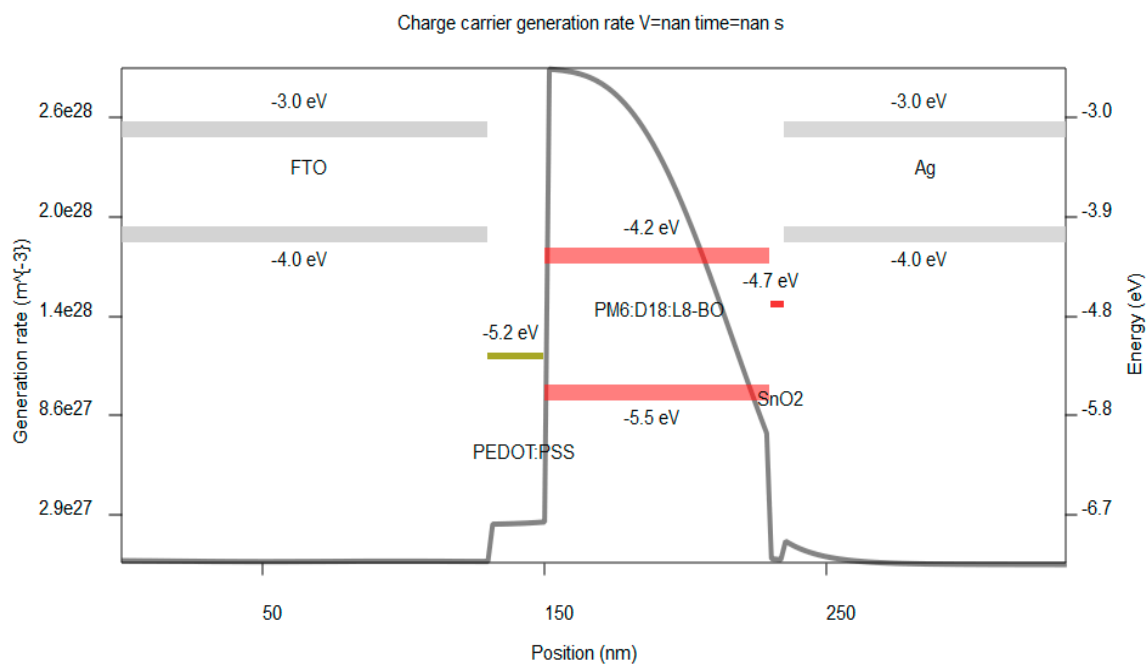


**Figure S7.** Charge carrier generation rate with energy level alignment of different materials of the Ternary device in function of position

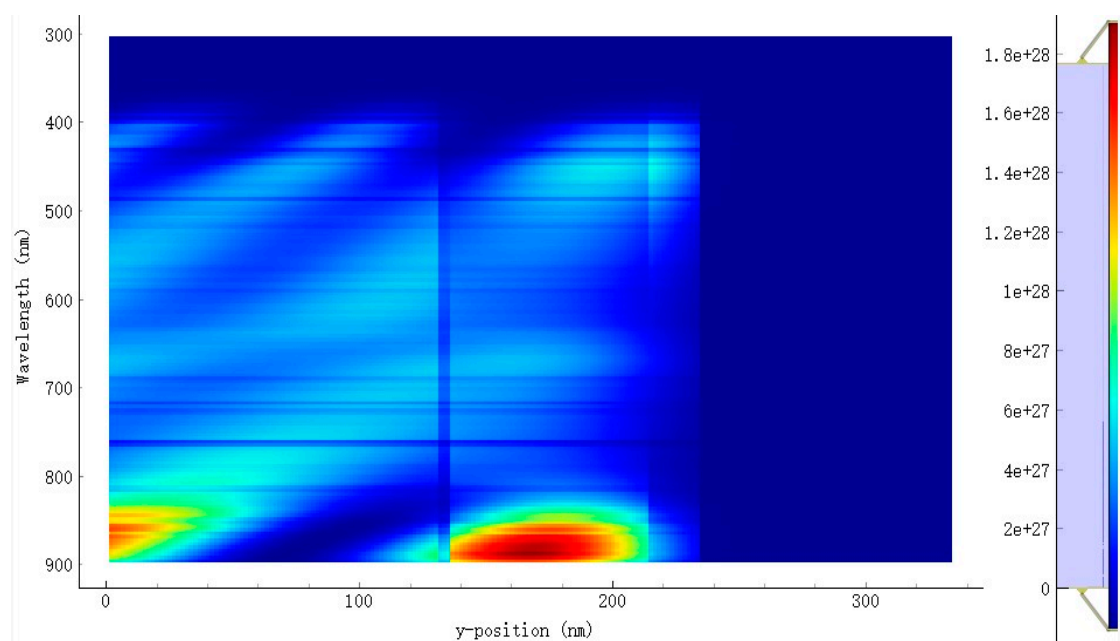


**Figure S8.** The distribution of the specterspecter of incident photons of the *D-A* active layer PM6:D18:L8-BO for conventional binary devices

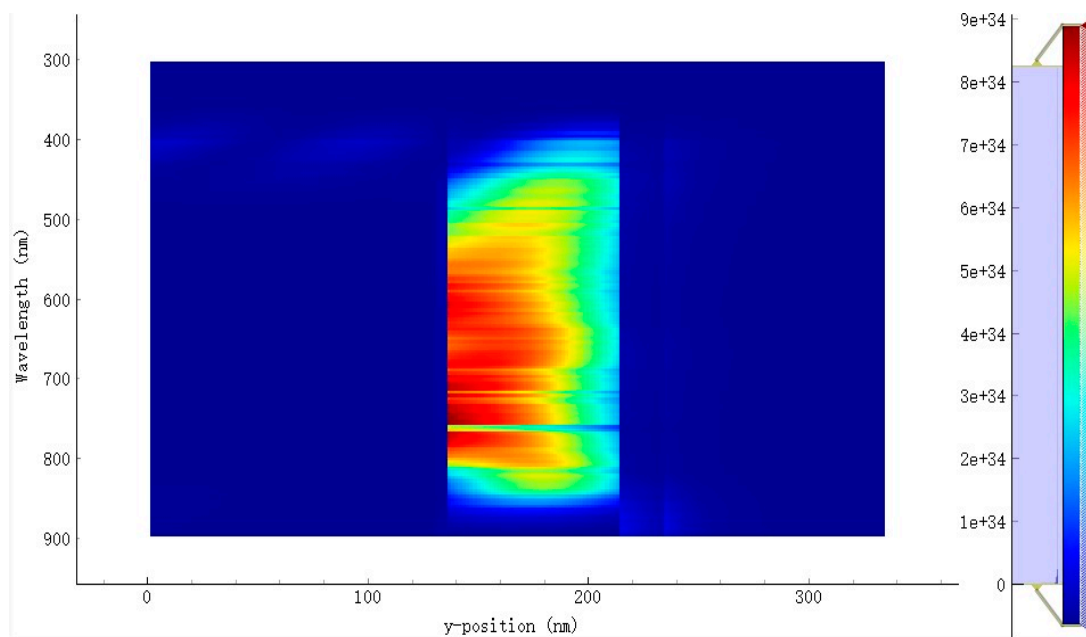


**Figure S9.** The distribution of the specter of the absorbed photons of the *D-A* active layer PM6:L8-BO for inverted binary device

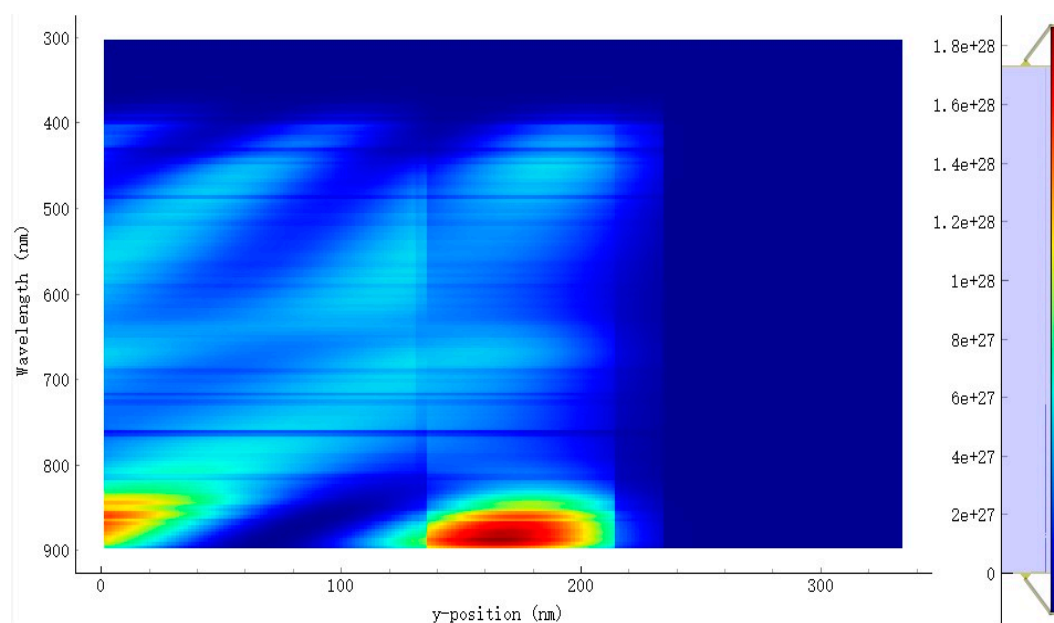


**Figure S10.** The distribution of the specter of the absorbed photons of the *D-A* active layer PM6:L8-BO for inverted binary device

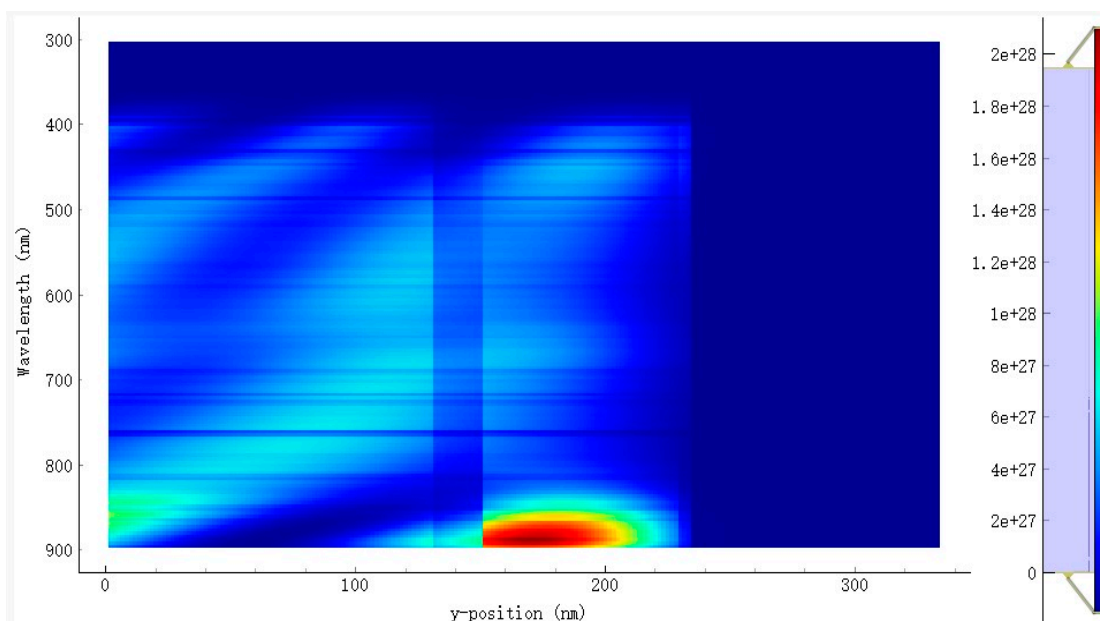


**Figure S11.** The distribution of the specterspecter of the absorbed photons of the *D-A* blend PM6:L8-BO for the Ternary device

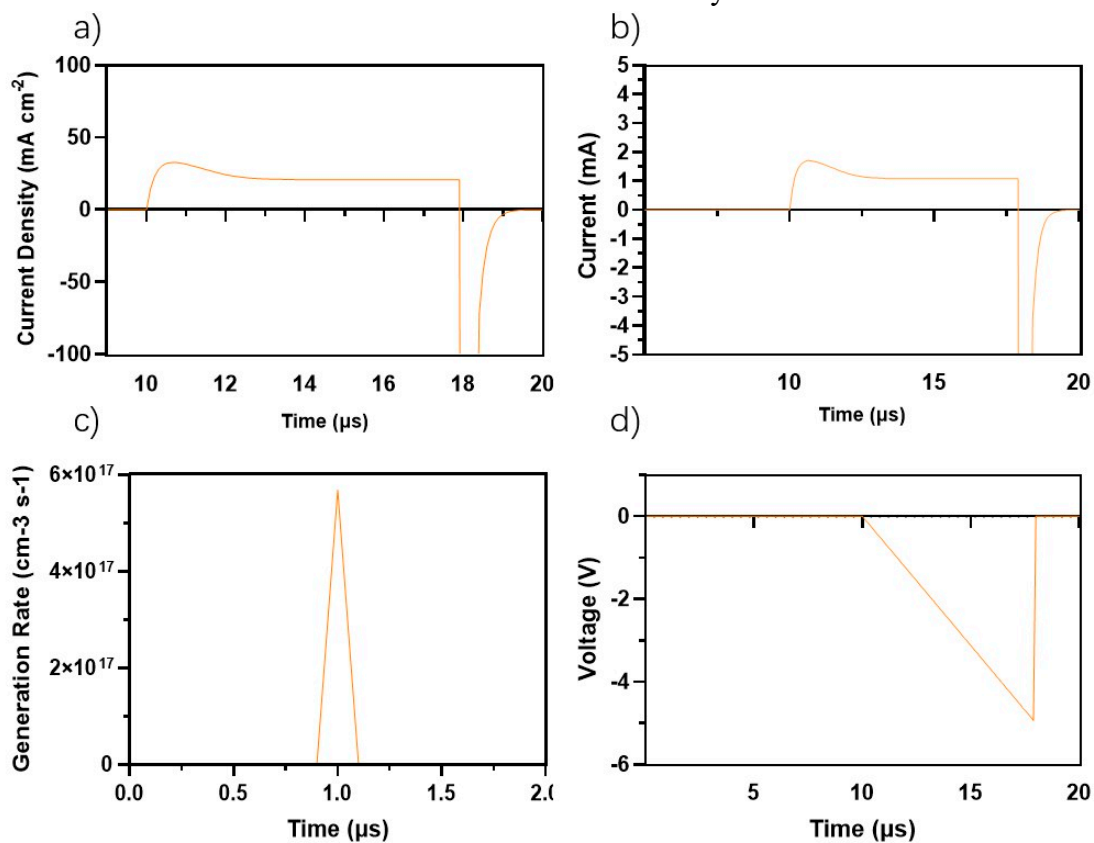


**Figure S12.** (a) transient current density for conventional binary devices; (b) transient current for for conventional binary devices; (c) transient generation rate for conventional binary devices; and (d) transient voltage for conventional binary devices



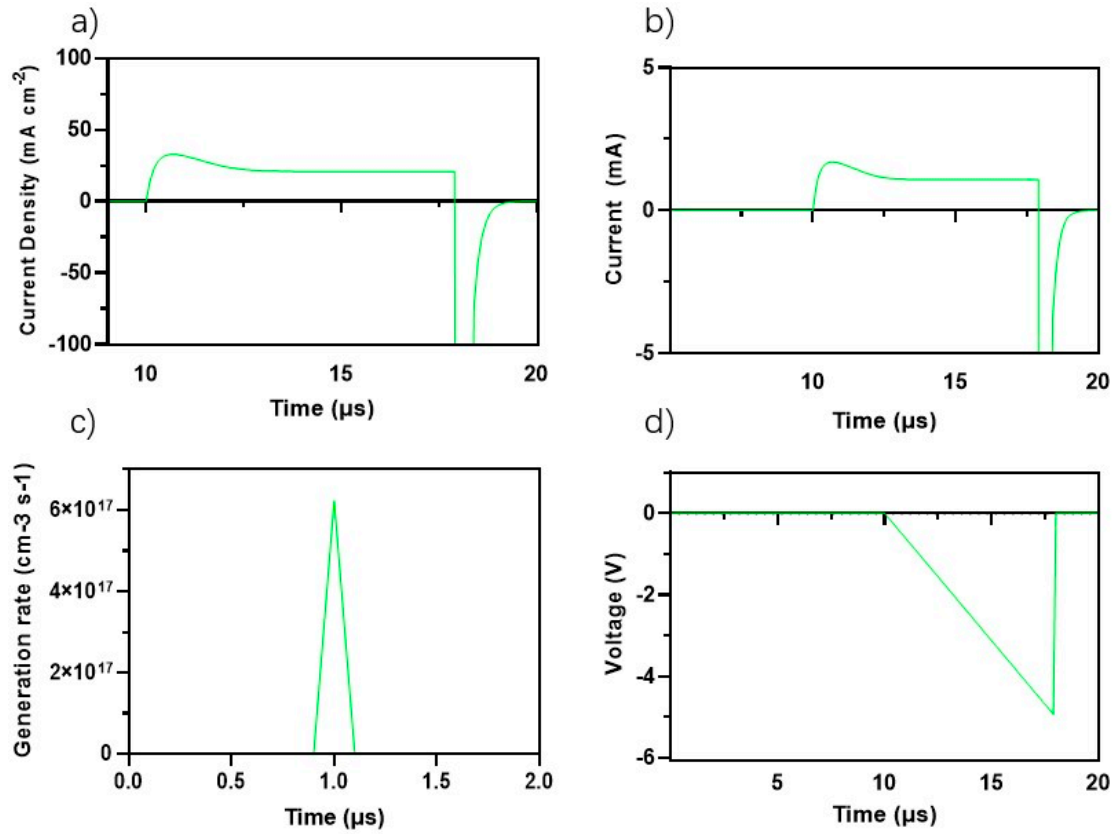


**Figure S13.** (a) transient current density for inverted binary devices; (b) transient current for the different mobilities for inverted binary devices; (c) transient generation rate for inverted binary devices; and (d) transient voltage for inverted binary devices

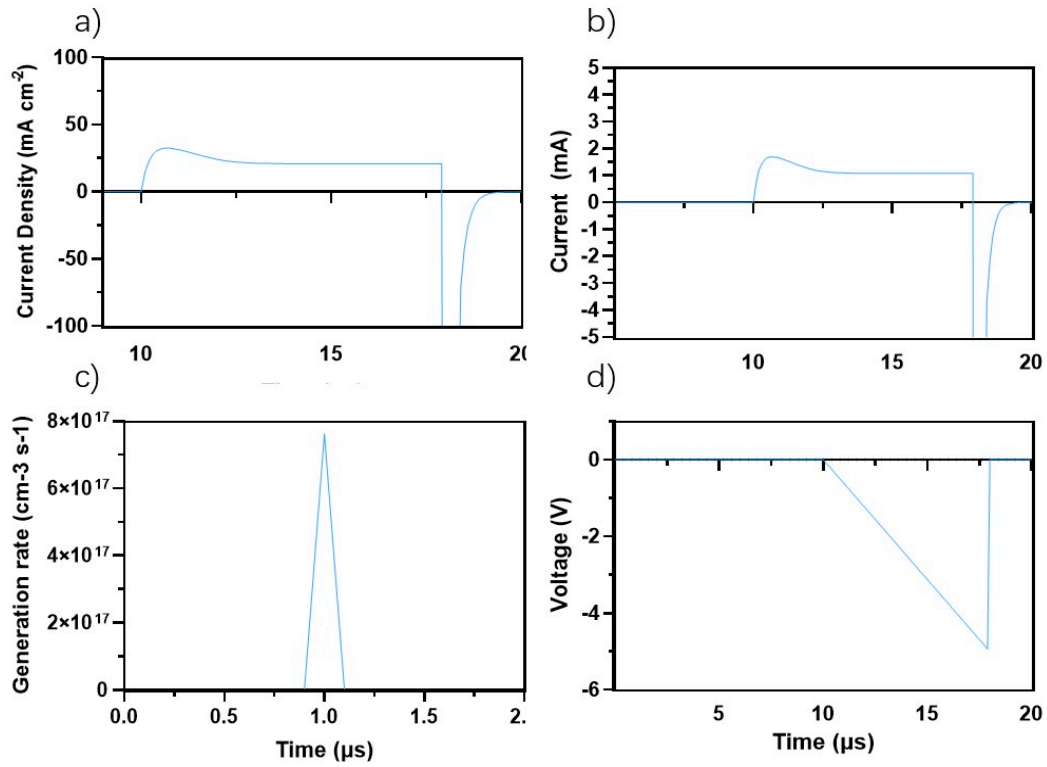


**Figure S14.** (a) transient current density for ternary; (b) transient current ternary devices; (c) transient generation rate for all devices; and (d) transient voltage for ternary devices

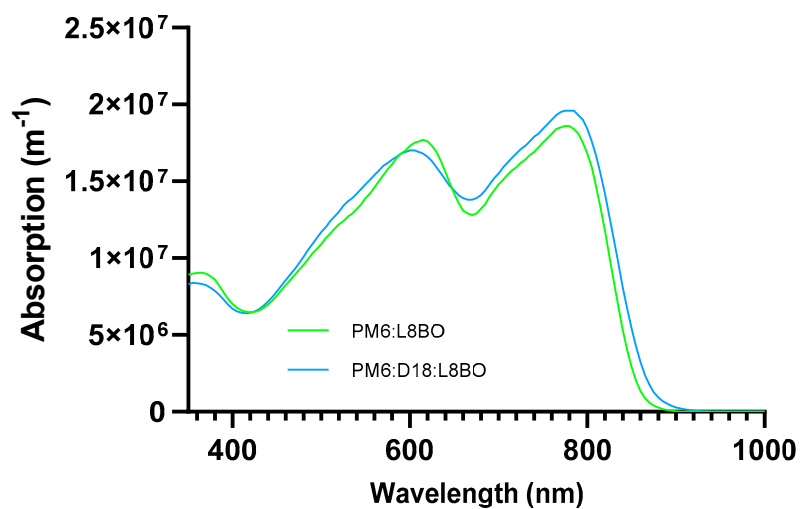


**Figure S15.** The absorption of light of the active layers PM6:L8-BO and PM6:D18:L8-BO.

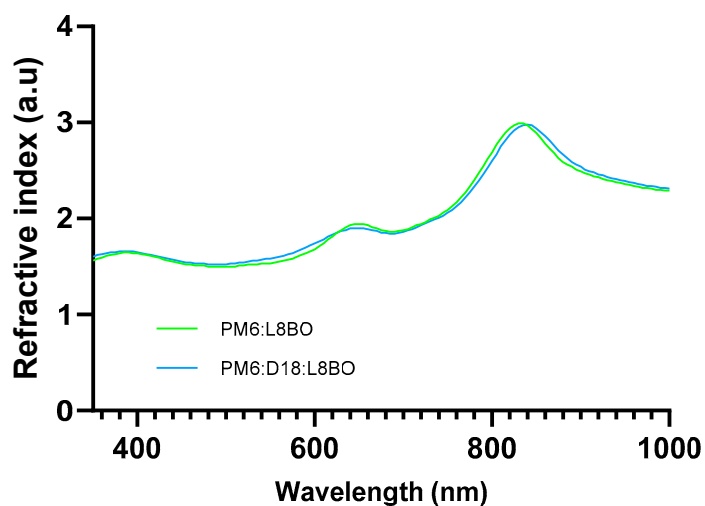


**Figure S16.** The refractive index of the active layers PM6:L8-BO and PM6:D18:L8-BO.

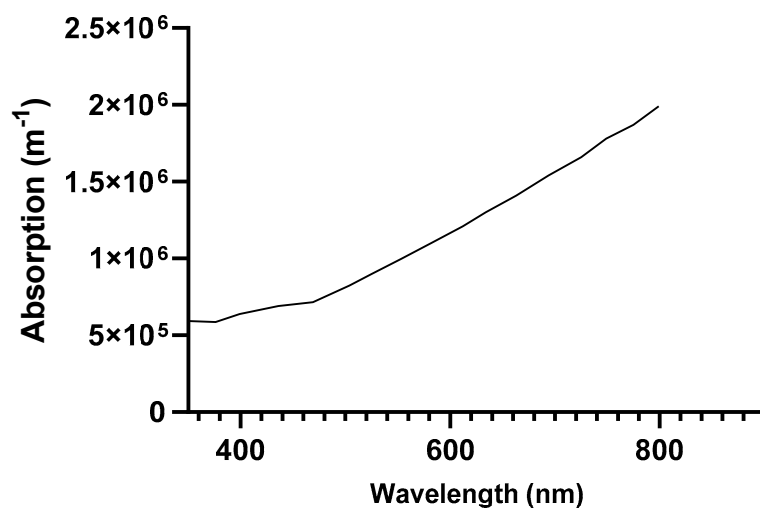


Figure S17. The absorption of light of PEDOT: PSS.

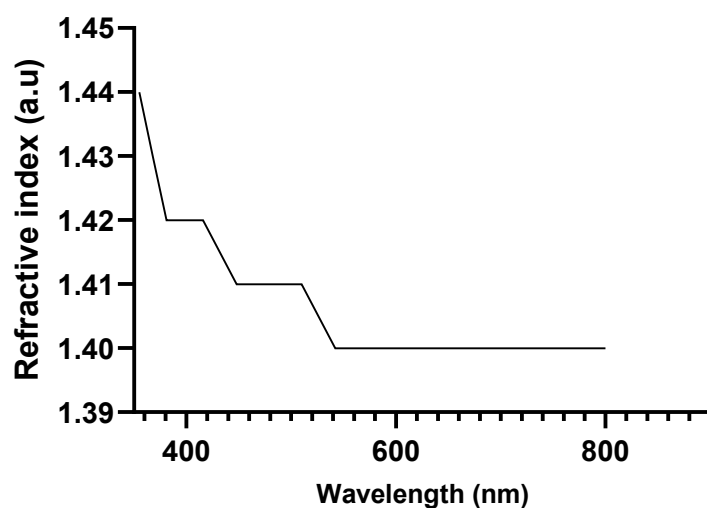


Figure S18. The refractive index of PEDOT: PSS.

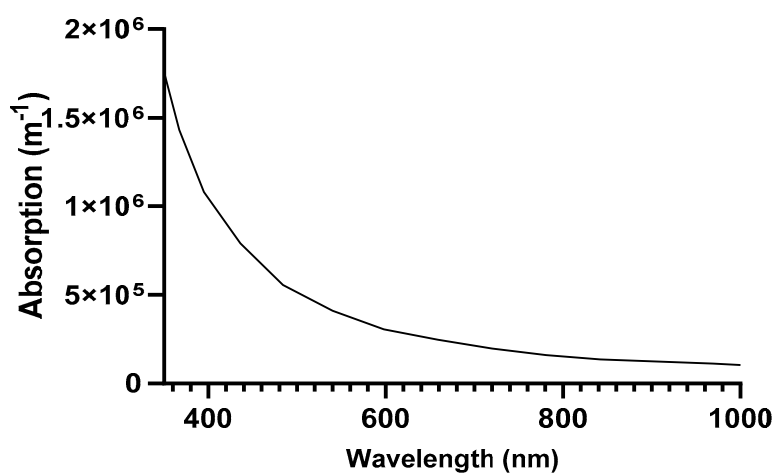


Figure S19. The absorption of light of SnO<sub>2</sub>.

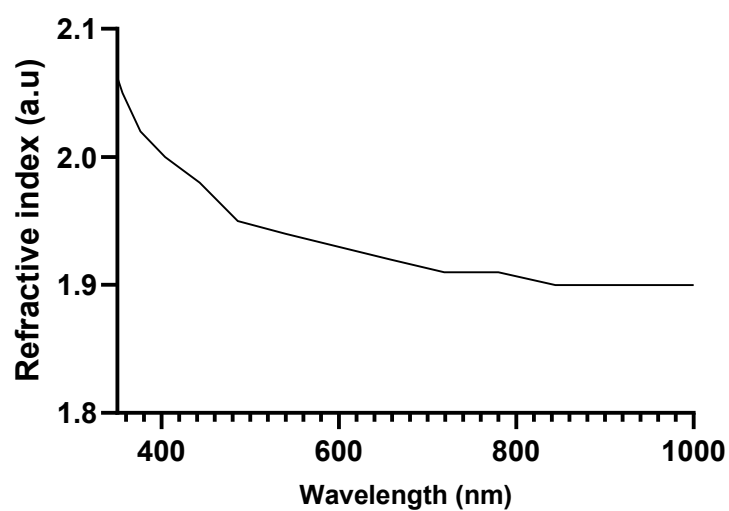


Figure S20. The refractive index of SnO<sub>2</sub>.

EQE and Integrated Jsc Curve

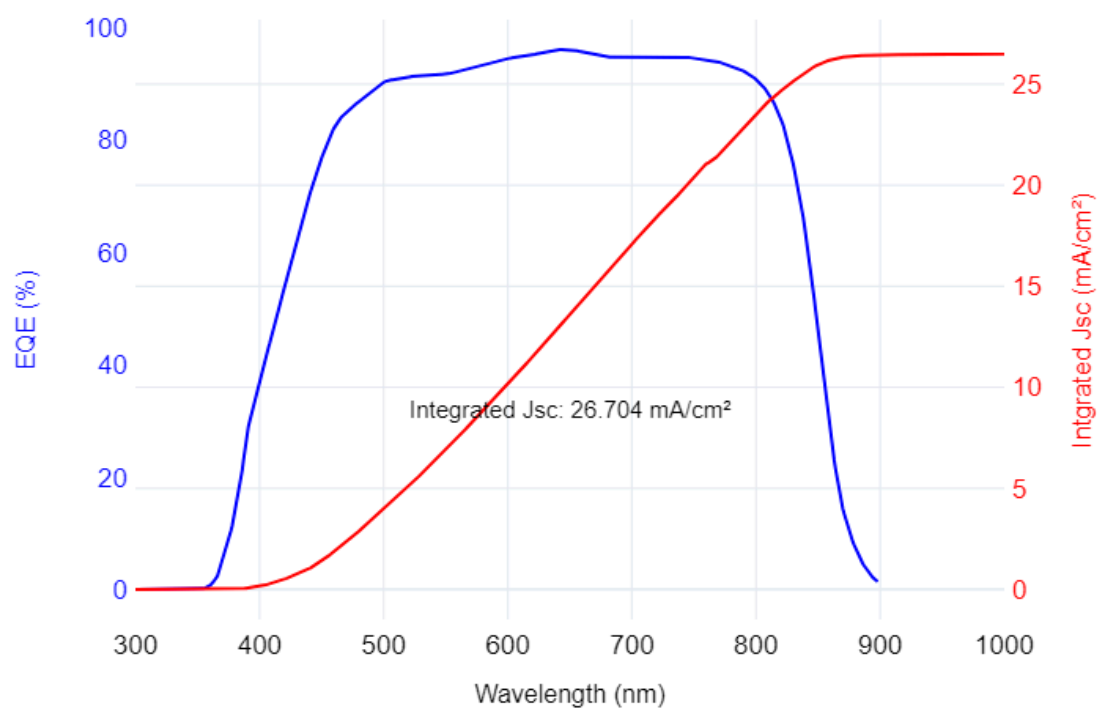


Figure S21. EQE and the integrated J<sub>sc</sub> curve of the direct binary device,

**EQE and Integrated Jsc Curve**

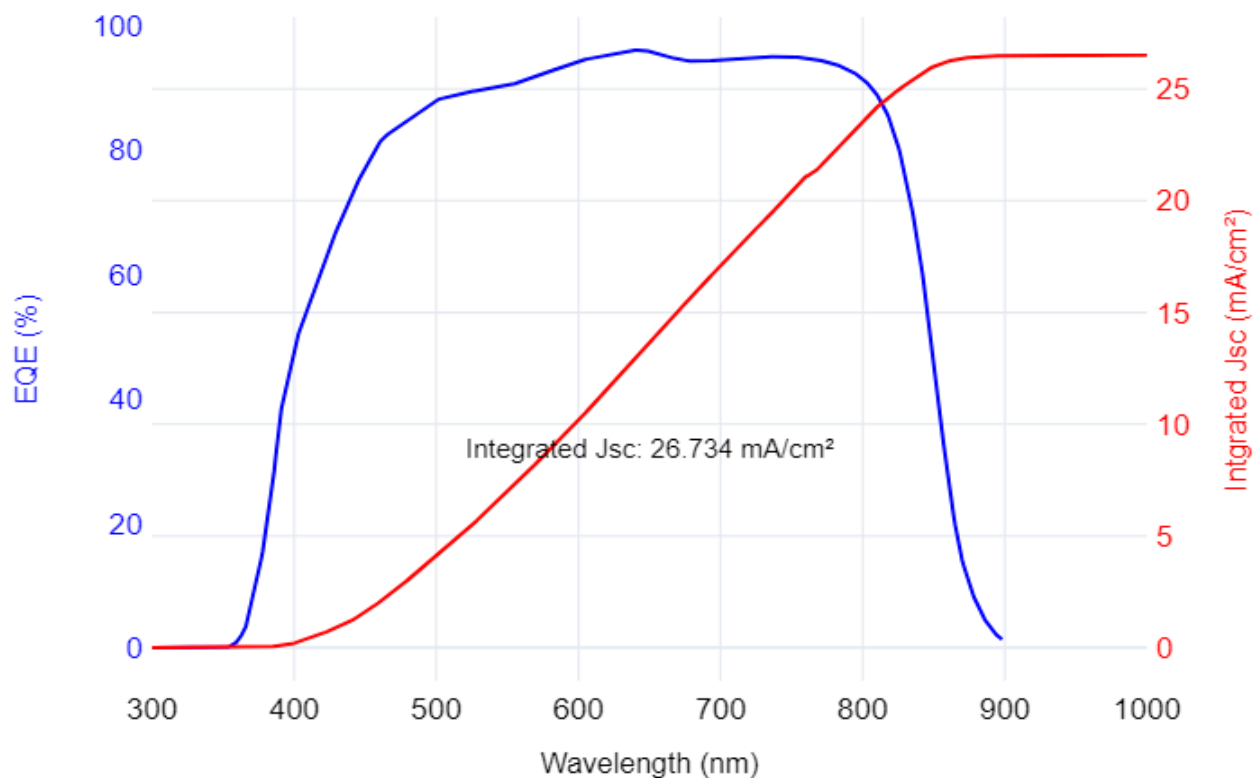


Figure S22. EQE and the integrated Jsc curve of the inverted binary device,

**EQE and Integrated Jsc Curve**

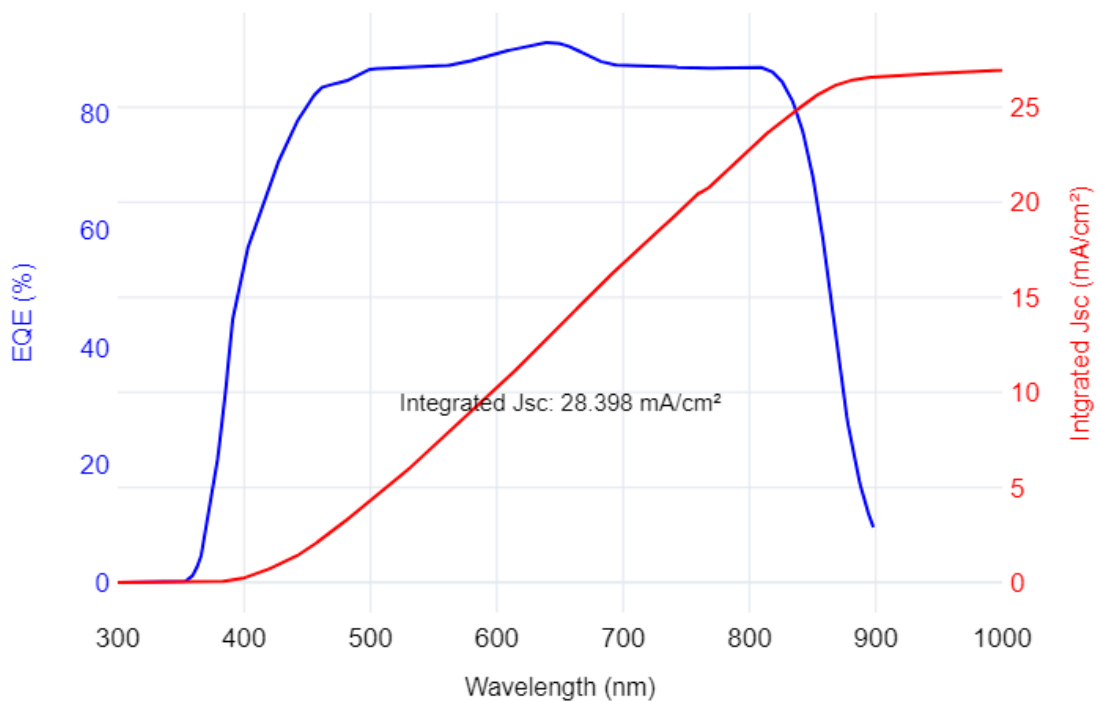


Figure S23. EQE and the integrated Jsc curve of the direct ternary device,